On the Catalytic Activity of $[RuH_2(PPh_3)_3(CO)]$ (PPh_3 = triphenylphosphine) in Ruthenium-Catalysed Generation of Hydrogen from Alcohols: a Combined Experimental and DFT study

Patrizia Lorusso,[a] Shahbaz Ahmad,[a] Karin Brill (née Schmid),[a] David J. Cole-Hamilton,[a] Nicolas Sieffert,*[b] and Michael Bühl*[a]

Dedicated to Prof. Alan Welch on the occasion of his retirement from Heriot-Watt University

Using density functional theory calculations (at the B97-D2//BP86 level) and measurements of kinetic isotope effects, we explored the mechanism of $[RuH_2(PPh_3)_3(CO)]$ (**22**) in catalytic acceptor-less dehydrogenation of methanol to formaldehyde. **22** is found to exhibit a similar activity as the previously studied $[RuH_2(H_2)(PPh_3)_3]$ (**1 b**) complex. On the computed pathway, $\eta^2 \rightarrow \eta^1$ slippage of Ru-bound formaldehyde prior to decoordination is indicated to be rate-limiting, consistent with the low k_H/k_D KIE of 1.3 measured for this reaction. We also explored computationally the possibility of achieving complete dehydrogenation of methanol (into CO_2 and H_2), through subsequent decarbonylation of formaldehyde and water-gas shift reaction of the resulting carbonyl complex. Complete pathways of this kind are traced for **22** and for $[RuH_2(PPh_3)_2(CO)_2]$. An alternative mechanism, involving a gem-diol intermediate (obtained upon attack of OH^- to coordinated formaldehyde), has also been investigated. All these pathways turned out to be unfavourable kinetically, in keeping with the lack of CO_2 evolution experimentally observed in this system. Our calculations show that the reactions are hampered by the low electrophilicities of the CO and HCHO ligands, making OH^- uptake unfavourable. Consequently, the subsequent intermediates are too high-lying on the reaction profiles, thus leading to high kinetic barriers and preventing full dehydrogenation of methanol to occur by this kind of mechanism.

Introduction

Regenerative biomass is an attractive source for the generation and storage of hydrogen gas (H_2), in the context of sustainable power management. In particular, if carbohydrates (such as cellulose) contained in plants could be fully decomposed into H_2 and CO_2, an overall "carbon-neutral" process could be envisaged, where the light harvesting apparatus of photosynthesis would be used to regenerate carbohydrates and consume the CO_2 produced in the first reaction. The resulting H_2 could fuel combustion engines or fuel cells, regenerating the water from which it was created. If such an overall sequence were possible, it would provide us with a more appealing way to produce hydrogen, compared to current industrial processes that are essentially based on fossil fuels as starting products. However, direct H_2 production from carbohydrates still remains challenging. Known reactions generally proceed *via* prior decomposition of the substrates.[1]

In this context, a significant research effort has been accomplished to design efficient (homogeneous) catalytic systems allowing for H_2 generation from carbohydrate derivatives, such as formic acid[2] or alcohols.[2b,3] Among them, methanol is a particularly attractive hydrogen source,[4] as it contains a higher hydrogen content than formic acid (12.5 wt% *vs* 4.3 wt%). In principle methanol can be catalytically dehydrogenated to three different products. Loss of one equivalent of H_2 gives formaldehyde (step *i* in Scheme 1), which could undergo subsequent reactions, e.g. to methyl formate.[5] Alternatively, the formaldehyde could be dehydrogenated to give a metal carbonyl complex and a second equivalent of H_2 (step *ii*). The carbonyl could be expelled from the metal as CO, possibly photochemically,[6] to regenerate the catalyst. Alternatively, it can be envisaged that the bound CO could undergo water gas shift reaction (WGSR) to give a third molecule of hydrogen and CO_2 (step *iii*).[7]

[a] Dr. P. Lorusso, S. Ahmad, K. Brill (née Schmid), Prof. D. J. Cole-Hamilton, Prof. M. Bühl
EastCHEM School of Chemistry
University of St. Andrews
North Haugh
St. Andrews, Fife KY16 9ST (UK)
E-mail: buehl@st-andrews.ac.uk
[b] Dr. N. Sieffert
Univ. Grenoble Alpes, CNRS, DCM
F-38000 Grenoble (France.)
E-mail: nicolas.sieffert@univ-grenoble-alpes.fr

Supporting information for this article is available on the WWW under https://doi.org/10.1002/cctc.202000159This publication is part of a Special Collection on "Phosphorus in Catalysis". Please check the ChemCatChem homepage for more articles in the collection.

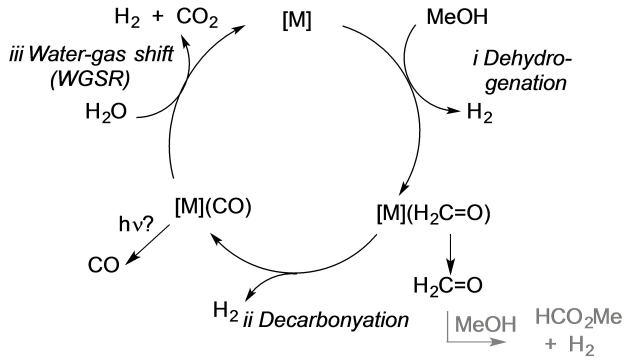

Scheme 1. Overall process under study for full decomposition of liquid methanol and water into gaseous H_2 and CO_2. [M] stands for a ruthenium complex acting as catalyst.

Proposed reaction sequence

These reactions are summarised along with their thermodynamic properties in equations (1)–(3) and Scheme 1:[8]

	ΔH° kJ/mol	ΔS° J/(K mol)	ΔG° kJ/mol	
$MeOH_{(l)} \rightarrow H_2CO_{(g)} + H_{2(g)}$	124	223	66.5	(1)
$MeOH_{(l)} \rightarrow CO_{(g)} + 2\,H_{2(g)}$	129	333	30	(2)
$MeOH_{(l)} + H_2O_{(l)} \rightarrow CO_{2(g)} + 3\,H_{2(g)}$	86	410	−36	(3)

Under standard conditions, only the reaction (3) is thermodynamically downhill, because of the formation of $CO_{2(g)}$. It is attractive for this reason, but also because it produces 3 moles of hydrogen per mole of methanol. The disadvantage is that all the carbon is "wasted" to CO_2. All of the possible reactions have positive entropy changes, so they become thermodynamically more accessible at higher temperatures.

Full decomposition of methanol could thus involve a sequence of three catalytic reactions, namely: *i.* dehydrogenation, *ii.* decarbonylation, and *iii.* WGSR (Scheme 1), affording the overall reaction (3).

Ideally, this sequence should be achieved using the same pre-catalyst, therefore allowing for a "one-pot" overall reaction. Such a process is expected in the dehydrogenation of ethanol catalysed by [Rh(bipy)]Cl_2 (bipy = 2,2′-bipyridyl).[9]

More recently, Beller[10] and Trincado and Grützmacher[11] reported the first examples of full decomposition of methanol involving Ru complexes bearing polydendate "pincer" ligands. These systems, however, do not involve WGSR but proceed *via* the formation of a gem-diol intermediate, further converted into formic acid and, finally, into hydrogen and carbon dioxide (see Scheme 2). Some other dehydrogenation catalysts reported in the literature only afford a single H_2 molecule per substrate molecule, and are thus unable to achieve the full decomposition of alcohols into H_2 and CO_2.[2b] Further developments in this field would benefit from a deeper understanding of the mechanisms underlying the catalytic reactions. The latter are multiple-step processes, and thus involve a broad number of short-lived intermediates that are challenging to characterize experimentally. As a result, detailed mechanistic information is still limited, and is essentially obtained with the help of computations.

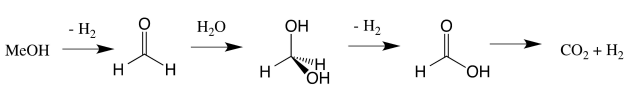

Scheme 2. Full decomposition of methanol via the formation of methanediol and formic acid.

We recently undertook a comprehensive mechanistic study of the catalytic system developed by Morton and Cole-Hamilton, involving the [$RuH_2(X_2)(PPh_3)_3$] (X_2=H_2 (**1 b**), PPh_3 or N_2) complexes as catalyst precursors. This system was among the first being very active for acceptor-less dehydrogenation of alcohols, and allows for an efficient conversion of aliphatic alcohols under basic conditions, at 150 °C.[12] Interestingly, the reaction rate increases with the length of the alkyl chain of the substrate (going from methanol to butanol), and the presence of complex **22** (resulting from decarbonylation, see Scheme 3) has been detected. **22** has been also be identified to be a catalyst for dehydrogenation in this system.[12] A series of [$RuH_2(X_2)(PPh_3)_3$] complexes was also considered regarding the overall sequence shown in Scheme 1, and their propensity to promote decarbonylation and WGSR reactions have been studied by measuring the quantity of produced CO, CH_4 (resulting from decarbonylation) and CO_2 (resulting from WGSR), during conversion of ethanol.[9] Interestingly, a significant amount of methane was produced, but no CO_2 has been detected (even after neutralisation of the solution with concentrated HCl). This revealed that the overall cycle shown in Scheme 1 should not be achievable with these pre-catalysts,

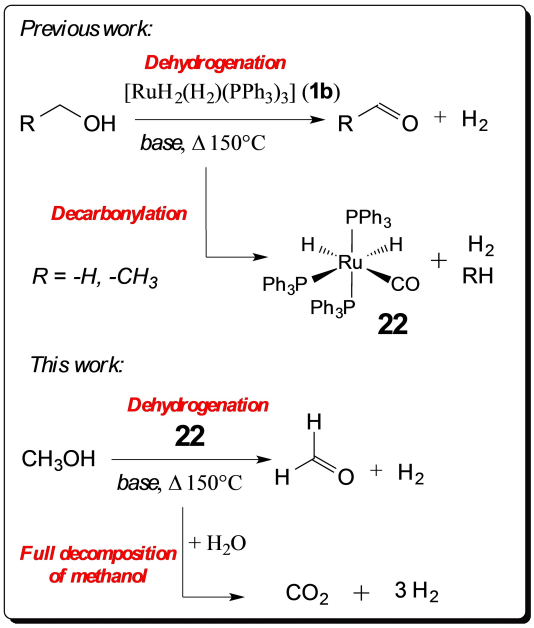

Scheme 3. The previously investigated dehydrogenation[13a] and decarbonylation[13b] of alcohols catalysed by [$RuH_2(H_2)(PPh_3)_3$] (**1 b**) and the newly investigated reactions regarding full decomposition of methanol catalysed by **22**.

since only steps 1 and 2 take place, but WGSR is not operating (step 3).

Our previous mechanistic investigations on this system[13] were based on Density Functional Theory (DFT) calculations, coupled to experimental determinations of Kinetic Isotope Effects (KIEs). In a first report, we focused on the dehydrogenation step itself (*i.e.* the first step of the overall cycle shown on Scheme 1), in which **1b** plays the role of pre-catalyst. We showed that the reaction mechanism is, in fact, complex, as four different reaction channels have been identified. The latter are strongly interlocked and possess close overall activation barriers. These results suggest that multiple reaction pathways should be considered to explain the reactivity of **1b** regarding dehydrogenation.[13a] In a second report, we focused on the decarbonylation reaction (*i.e.* the second step of the cycle shown in Scheme 1), leading to the formation of the carbonyl complex **22**. We proposed a detailed mechanism for decarbonylation and we found that the latter is indeed kinetically facile with methanol and ethanol substrates. The overall activation barriers are found to be close to the one for dehydrogenation, indicating that the two reactions should be competitive. Also, a significant driving force was found for the formation of **22**.[13b] Interestingly, a kinetic isotope effect has been measured for a decarbonylation pathway, suggesting that the rate-limiting step is the first α-H abstraction from the coordinated formaldehyde (namely, the dehydrogenation product of methanol), in keeping with our computational results.[13b] Very recently, some of us characterized isotopomers of **22** (obtained from reaction between **1b** and CD_3OD in presence of Na) by ^1H NMR,[14] and showed that their relative population in solution is consistent with one of the decoordination pathways (pathway **G**) that has been previously established from computations.[13b] A summary of pathways **A**–**G**, as obtained in our previous studies, is provided in supporting information (see Scheme S1).

Herein, we extend our mechanistic studies to explore the reactivity of **22** in the catalytic system (see Scheme 3). First, we investigate its potential role as dehydrogenation catalyst precursor, *i.e.* ensuring step 1 of the overall cycle shown in Scheme 1, with [M]=[$RuH_2(PPh_3)_2(CO)$]. We report a detailed mechanism describing its reactivity towards methanol, considering that the carbonyl ligand remains coordinated in all intermediates involved in the catalytic cycle. The results of the experimental determination of Kinetic Isotope Effects (KIE) are also presented. Next, we explore the propensity of **22** to undergo WGSR (*i.e.* corresponding to the third step of the overall cycle shown in Scheme 1, with [M]=[$RuH_2(PPh_3)_2(H_2)$]), with the aim to better understand what are the limiting factors that prevent this reaction, as no CO_2 evolution is found for this catalyst.[9] For completeness, the possibility of a gem-diolate pathway (GDP) mechanism was as also considered (i.e. involving the sequence described in Scheme 2). Finally, we investigated the viability of a full catalytic cycle allowing for full decomposition of methanol, as shown in Scheme 1, considering **22** as pre-catalyst.

Results

This section is organized as follows: first, we report DFT and experimental results on the propensity of **22** to catalyse methanol dehydrogenation. Next, we describe DFT results on CO_2 evolution involving **22**, considering both WGSR (third step of the overall cycle described in Scheme 1) and GDP. Finally, DFT results on the full decomposition of methanol involving **22** as pre-catalyst (see Scheme 1) are presented.

In pathways involving diphosphine complexes, two variants were considered, differing in the relative position of PPh_3 and CO ligands at the metal centre, so that a first mechanism involves isomers where the two ligands are in axial positions, while the second mechanism involves isomers where PPh_3 is in an axial position and CO is equatorial. For simplicity only the most favourable variant of each path is presented in the text, the other pathways, labelled with primes, are provided in the Supporting Information (ESI).

In all pathways considered herein, we assume that ligand exchange reactions follow a fully dissociative mechanism, i.e. taking place *via* the formation of five-coordinate Ru(II) complexes. Also, the latter are assumed to undergo facile isomerisation, by intramolecular rearrangement via turnstile- or pseudo-rotation.[15]

The labelling of all species and pathways reported herein are continuing those of our two preceding studies, focused on the dehydrogenation (pathways **A**–**D**)[13a] and decarbonylation (pathways **E**–**G**; see also Scheme S1 for details)[13b] reactions. Consequently, the labelling of new species starts with 32. When applicable, the "a" and "b" suffixes denote classical and non-classical hydrides, respectively, whereas the "ax" subscript refers to stereoisomers where PPh_3 and CO are both in axial positions.

After a detailed description of the catalytic cycles, their kinetics is analysed compared to the previously established mechanisms.[13] Additionally, the results of CH_3OH/CD_3OD competition experiments for the determination of the rate-limiting step of methanol dehydrogenation catalysed by **22** are presented, along with a comparison between experimental and computed KIEs.

Unless otherwise specified, all energies mentioned in the text are free energies computed at the B97-D2/ECP2 level and corrected for basis set superposition error (BSSE, see Eq. (8) in Computational details). The model solvent is methanol and the temperature is 150 °C throughout. Free energies of every elementary step are gathered in Tables S1 and S3–S7.

I. Methanol dehydrogenation catalysed by [$RuH_2(PPh_3)_3(CO)$] (22)

Description of pathway H, established from DFT calculations

Based on the reaction pathway **C** previously reported for alcohol dehydrogenation catalysed by [$RuH_2(H_2)(PPh_3)_3$] (**1b**),[13a] we investigated an analogous path, denoted **H** (Figure 1), for methanol dehydrogenation catalysed by complex **22**, in which all intermediates feature a (single) carbonyl ligand. The active

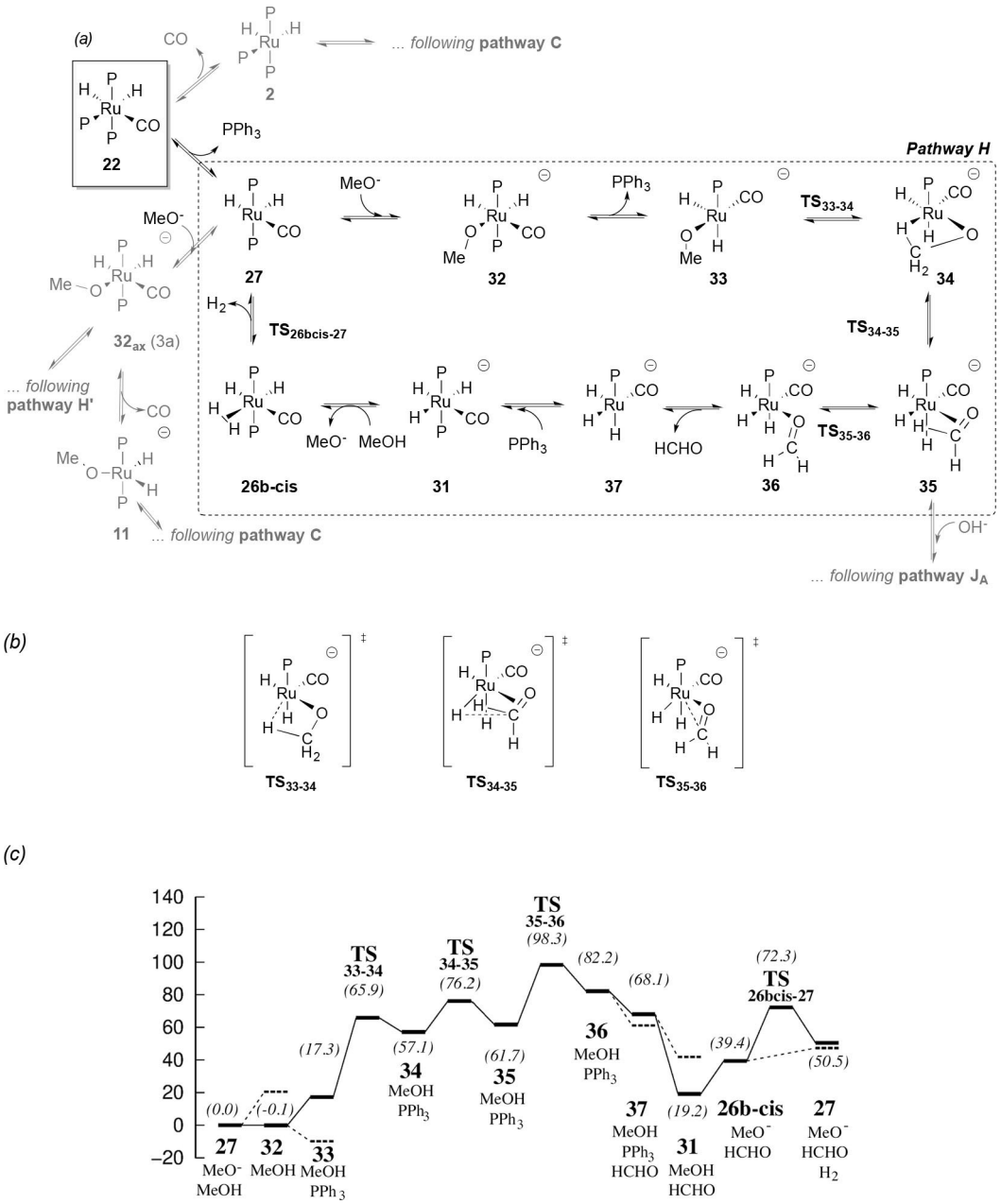

Figure 1. Dehydrogenation pathway **H** (catalysed by **22**) and its link to dehydrogenation pathway **C** (catalysed by **1b)** previously studied (see reference[13a]). A link towards the GDP pathway **Cycle-2** (fully described in Scheme 6, Figures 4 and 5) is also shown. Schematic representation of: *(a)* intermediates and *(b)* transition states (P=PPh_3); *(c)* free-energy profile [kJ/mol], with calculations carried at the B97-D2/ECP2 level of theory using methanol as the model solvent. The dashed lines indicate BSSE-corrected free energies. Relative free energies (without correction for BSSE), using **27** as reference, are given in parentheses. Reaction energies for every individual step are given in Table S1.

species **27** can arise from **22** (which acts as a catalyst precursor) by dissociation of a phosphine ligand. This initiation step is found to be only moderately unfavourable thermodynamically (by 52.3 kJ/mol at the ECP2 level and 43.6 kJ/mol at the ECP3 level; see Tables S1 and 1, respectively), suggesting that intermediate **27** should still be present to a small extent in the catalytic system. Since the dehydrogenation reaction occurs under basic conditions,[12] **27** can coordinate MeO^- to afford the anionic methoxy intermediate **32**.[16] This step is thermodynamically uphill ($\Delta G_{27\rightarrow32}=20.5$ kJ/mol), but the subsequent dissociation of the phosphine ligand can easily occur ($\Delta G_{32\rightarrow33}=-9.7$ kJ/mol). This process affords the five-coordinate species **33** *via* a reorganisation of the methoxy, carbonyl and hydrido ligands.

Species **33** undergoes β-H abstraction, via the formation of the agostic intermediate **34** ($\Delta G_{33\rightarrow34}=39.7$ kJ/mol and $\Delta G^{\neq}_{33\rightarrow34}=48.6$ kJ/mol). The subsequent breaking of the C–H bond affords intermediate **35**, where the HCHO product is π-coordinated to the metal ($\Delta G_{34\rightarrow35}=4.7$ kJ/mol and $\Delta G^{\neq}_{34\rightarrow35}=19.1$ kJ/mol). The decoordination of the formaldehyde product

to generate **37** is facile (overall $\Delta G_{35\rightarrow37} = -0.5$ kJ/mol) and takes place in two steps. First, intermediate **36**, where the HCHO ligand is η^1-coordinated to the metal centre, is afforded. Next, HCHO decoordinates to afford **37**. The $\eta^2\rightarrow\eta^1$ slippage of formaldehyde is rate-limiting ($\Delta G_{35\rightarrow36} = 20.5$ kJ/mol and $\Delta G^{\neq}_{35\rightarrow36} = 36.6$ kJ/mol), as observed in our previous studies on methanol dehydrogenation[13a] and decarbonylation.[13b] The formation of **31** is thermodynamically favourable ($\Delta G_{37\rightarrow31} = -26.3$ kJ/mol). Note that, in this pathway, recoordination of the phosphine occurs *via* a rearrangement of the first coordination sphere, where a hydride ligand moves from an axial to an equatorial position. The resulting trihydride complex **31** can be further protonated by methanol to afford the non-classical hydride **26b–cis**. Finally, loss of H_2 from the latter allows for the regeneration of **27**. We note that these latter steps (**31**→**26b–cis**→**27**) are also involved in the methanol decarbonylation pathway **G**, and have been described in detail in reference.[13b] The same sequence of elementary steps is obtained in pathway **H′**, described in Figure S1 and Table S1 in the ESI.

Kinetics of the dehydrogenation pathway H and comparisons with the previously studied pathway C (DFT results)

In order to compare the kinetics of pathways **H** (and **H′**) to the ones previously described,[13] the initiation steps and overall activation barriers have been recomputed at the higher ECP3 level of theory, as done previously.[13] The BSSE corrections (noted $\delta E'_{BSSE}$) were recalculated using a more elaborated approach, allowing for a better estimation of the error when the (de)coordination of more than one ligand is occurring during the overall reaction (see Section II.2 in the ESI for details). All energy components (except δE_G) to the overall free energies were recomputed at the B97-D2/ECP3 level, and are reported in Table 1.

The overall activation energy computed for pathway **H** is 114.2 kJ/mol (see Table 1), *i.e.* comparable with (and even slightly lower than) that for the analogous path **C** (131.0 kJ/mol).[13] Pathway **H′** appears to be somewhat less favourable (overall barrier 134.9 kJ/mol). Our DFT results thus confirm that complexes **1b** and **22** should both be catalysts for methanol dehydrogenation with comparable activity, and that **22** could potentially be even slightly more active than **1b**. Interestingly, while a switch from pathway **C** to **H** is possible through decarbonylation forming **22**,[13b] the reverse is not possible because of the high thermodynamic stability of the carbonyl complexes. For instance, switching from intermediate **32** on path **H** to intermediate **11** on path **C** (through CO dissociation) would require an overall free energy barrier of $\Delta G^{\neq} = 245.8$ kJ/mol to be overcome to achieve turnover (via subsequent $\mathbf{TS_{13-14}}$, see Table 1). Such a barrier should certainly be out of reach under actual reaction conditions.

Experimental determination of H/D KIE and comparison with DFT results

The experimental H/D KIE for methanol dehydrogenation catalysed by **22** (pathways **H** and **H′**) could be estimated by following the destiny of the formaldehyde product, bearing in mind the "one-pot" catalytic system we have proposed in reference,[17] where the formaldehyde obtained as a product of

Table 1. Refined free energies (in kJ/mol at the B97-D2/ECP3 level) for initiation steps and overall activation barriers.

		ΔE_{gas}	$\delta E'_{BSSE}$	δE_{Solv}	δE_G	ΔG
	Overall reaction free energies					
	$MeOH + H_2O \rightarrow 3\ H_2 + CO_2$	60.6	0.0	38.1	−89.4	9.3
	$2\ MeOH + OH^- \rightarrow 3\ H_2 + CO_2 + MeO^-$	26.8	0.0	105.5	−101.5	30.7
	Initiation free energies					
C[a]	**22**→**2** + CO	194.7	−12.3	3.2	−58.3	127.3
H/H′	**22**→**27** + 2 PPh_3	241.4	−31.9	−70.8	−95.2	43.6
$\mathbf{G_{CO}}$	**22** + MeO^- → **55** + 2 PPh_3 + H_2	90.0	−39.1	40.3	−155.9	−64.8
$\mathbf{G'_{CO}}$	**22** + MeO^- → **55ax** + 2 PPh_3 + H_2	112.5	−39.2	−37.2	−156.8	−46.3
$\mathbf{G_{CO}}$	**22** + MeOH → **58** + 2 H_2 + PPh_3	147.5	−23.5	−1.9	−136.0	−13.9
$\mathbf{G'_{CO}}$	**22** + MeOH → **58ax** + 2 H_2 + PPh_3	143.2	−18.4	−1.3	−130.3	−6.8
	Overall free energy barriers					
C[b]	**1b** + MeO^- → $\mathbf{TS_{13-14}}$ + H_2 + PPh_3	118.0	−21.8	119.7	−84.9	131.0
C[a]	**22** + MeO^- → $\mathbf{TS_{13-14}}$ + CO + PPh_3	253.5	−31.9	122.3	−98.2	245.8
H	**22** + MeO^- → $\mathbf{TS_{35-36}}$ + 2 PPh_3	246.3	−38.7	18.9	−112.4	114.2
H′	**22** + MeO^- → $\mathbf{TS_{35ax-36ax}}$ + 2 PPh_3	264.9	−38.3	23.5	−115.2	134.9
I	**22** + OH^- → $\mathbf{TS_{40-41}}$	−65.8	7.7	209.8	32.8	184.5
	Free energy spans for full decomposition of methanol					
Cycle-1	**22** + OH^- + MeOH → $\mathbf{TS_{13-28}}$ + H_2 + PPh_3 + CO_2	124.2	−29.8	212.5	−99.3	207.6
Cycle-2	**22** + MeOH + OH− − → $\mathbf{TS_{44-45}}$ + 2 PPh_3	139.9	−31.2	141.7	−84.2	166.1
Cycle-2′[c]	**22** + MeOH + OH^- → $\mathbf{TS_{44ax-45ax}}$ + 2 PPh_3	154.6	−31.4	145.0	−88.0	180.2
Cycle-3	**55** + 2 MeOH + OH^- → $\mathbf{TS_{51-52}}$ + MeO^- + CO_2 + 2 H_2	154.7	2.8	115.0	−64.4	208.1
Cycle-3′[d]	**55ax** + 2 MeOH + OH^- → $\mathbf{TS_{35ax-51ax}}$ + MeO^- + CO_2 + 2 H_2	161.2	0.3	97.3	−61.6	197.2

[a] Considering an entry to pathway **C** via CO decoordination from **22**. [b] from reference.[13a] [c] Analoguous to ***Cycle-2***, but involving pathways **H′**, $\mathbf{J'_A}$ and $\mathbf{J'_B}$. [d] Analoguous to ***Cycle-3***, but involving pathways **H′**, $\mathbf{G'_{CO}}$ and $\mathbf{I'_{CO}}$.

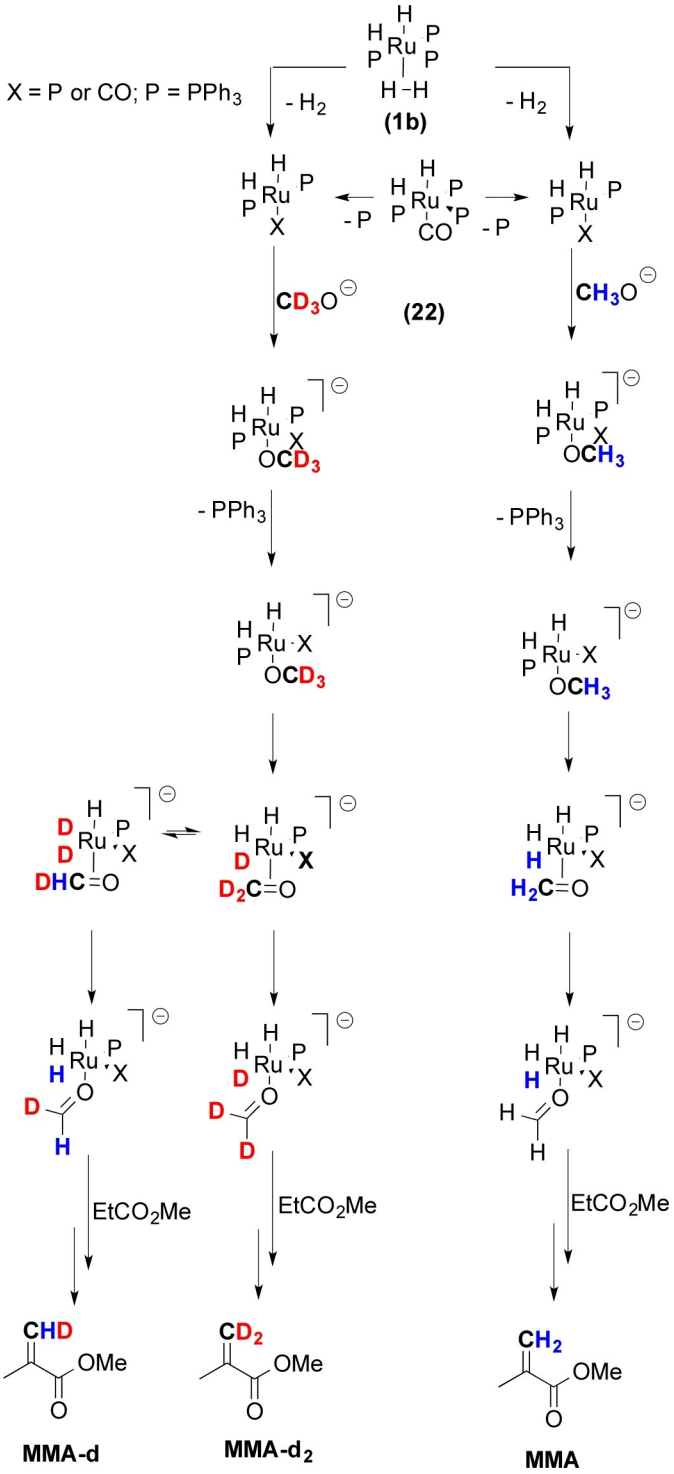

Scheme 4. Overview of the reaction intermediates involved in the formation of MMA, MMA-d and MMA-d_2 when starting from catalyst **22** or **1b** (P=PPh_3).

methanol dehydrogenation can undergo condensation with α-deprotonated methyl propanoate to afford methyl methacrylate (referred to as MMA). A similar scenario should be observed when starting from complex **1b**, since we have shown that both species, **22** and **1b**, act as catalyst precursors generating *in situ* the active five-coordinate species **27** or **2** respectively, subsequently involved in the mechanism previously investigated (see pathways **A**–**C** from ref.[13a] and pathway **H** presented in Figure 1).

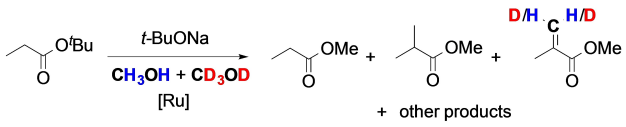

Scheme 5. General reaction conditions for the one-pot system depicted above: cat. 1 (0.124 g, 0.135 mmol), *t*-BuP (15.64 mL, 103.9 mmol), *t*-BuONa (2.6 g, 27.0 mmol), toluene (10 mL), methanol (3.8 mL, 93.5 mmol), methanol-d4 (3.8 mL, 93.5 mmol), 2,4-dimethyl-6-tert-butylphenol (Topanol A, 0.01 mL). Hastelloy™ autoclave; 170 °C under an atmosphere of ethene (6 bar) for 3 h.

When the reaction is performed using equal amounts of CH_3OH and CD_3OD, the formation of non-deuterated and bis-deuterated formaldehyde should be observed. The latter compound, in turn, can undergo intramolecular H/D exchange to generate the mono-deuterated derivative. The three isotopomers, CH_2O, CHDO and CD_2O, once involved in the subsequent condensation step will afford the non-, mono- and bis-deuterated MMA (namely, MMA, MMA-d and MMA-d_2). The ratio of [MMA : (MMA-d + MMA-d_2)] can be directly related to the H/D KIE (see Scheme 4).

To determine the deuterium isotope effect, the reaction was carried out using *tert*-butyl propanoate (*t*-BuP) as substrate and sodium *tert*-butoxide (*t*-BuONa) as base (so that the only source of methanol/methoxide was the added methanol) and equal amounts of CH_3OH and CD_3OD (see Scheme 5 for detailed reaction conditions). The crude product was analysed via GC-MS spectroscopy.

The analysis of the $[M–OMe]^+$ fragment of MMA (peaks at 69, 70 and 71 m/z respectively depicted in Figure 2), showed that the methylene group contained zero (56.3%), one (23.0%) or two (20.7%) deuterium atoms. By assuming that the contribution of the non-deuterated species to the peak at 70 m/z is negligible, these percentages could be used to determine the ratio of [MMA : (MMA-d + MMA-d_2)] that directly equates to a kinetic isotope effect (k_H/k_D) of 1.3 for the dehydrogenation pathway under study. This result is in good agreement with the computed values (as obtained from free energies of activation, see Table 2), which are 1.3 for pathway **H** and 1.9 for pathway **C**[13a] (see Table 2), *i.e.* considering either **22** or **1b** as pre-catalyst, respectively.

Such very small H/D KIEs typically arises from isotopic substitution at a bond that does not undergo cleavage during the rate-determining step (secondary kinetic isotope effect),[18] in good accordance with our DFT results where the highest barrier corresponds to the partial decoordination of the formaldehyde product, while much larger values of the order of 6 or more denote the breaking or formation of C–H bonds in the rate-determining step.

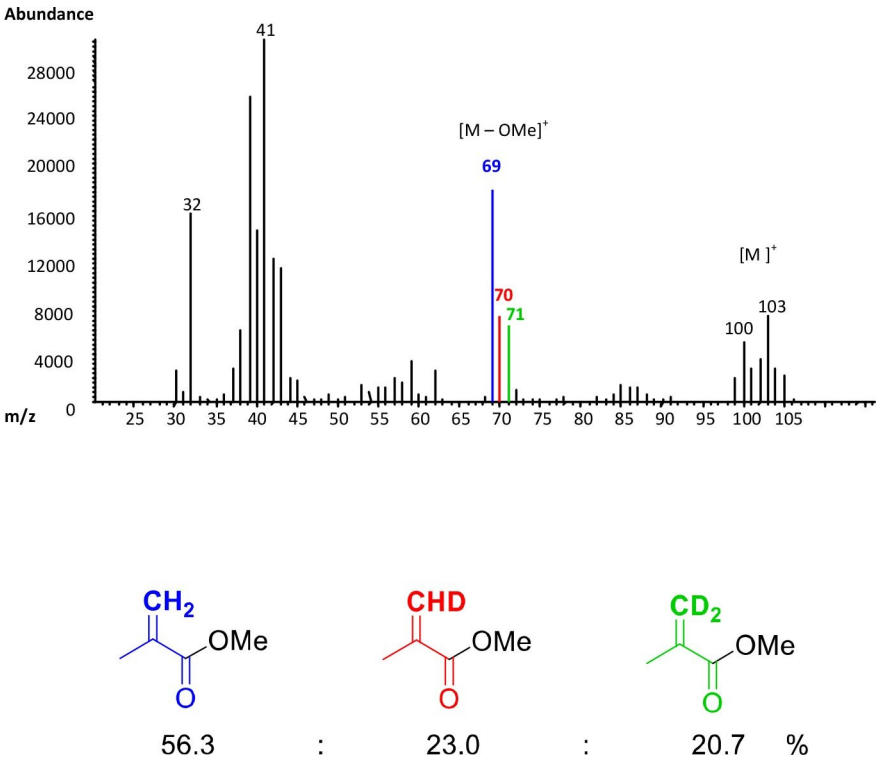

Figure 2. Fragmentation pattern of MMA highlighting the fragment $[M-OMe]^+$. The peaks at 69, 70 and 71 m/z correspond to the non-, mono- and bis-deuterated MMA in the ratio of 56.3 : 23.0 : 20.7 % respectively.

Table 2. H/D KIEs determined computationally and experimentally.

	Rate-determining step	Computed $^1H/^2H$ KIE[a]	Experimental $^1H/^2H$ KIE
H	$\eta^2 \rightarrow \eta^1$ slippage of HCHO **22** + $MeO^- \rightarrow$ **TS**$_{3536+}$ 2 PPh_3	1.3 (1.7)	1.3
H′	$\eta^2 \rightarrow \eta^1$ slippage of HCHO **22** + $MeO^- \rightarrow$ **TS**$_{35ax-36ax+}$ 2 PPh_3	1.7 (2.0)	1.3
C	$\eta^2 \rightarrow \eta^1$ slippage of HCHO **1b** + $MeO^- \rightarrow$ **TS**$_{1314+}$ H_{2+} PPh_3	1.9 (4.4) [b]	–

[a] KIE computed at the RI-BP86/ECP1 level of theory at T = 423 K and P = 1354 atm by substituting all hydrogens, except phenyl hydrogens, with deuterium. Values computed from free energies (values computed from enthalpies are in parenthesis). See Table S2 for details; values of the imaginary frequencies for **H**, **H′** and **C** are 328*i* cm^{-1}, 235*i* cm^{-1} and 238*i* cm^{-1}, respectively, for transition states involving ^1H, and are *279i* cm^{-1}, *191i* cm^{-1} and *200i* cm^{-1}, respectively, for the deuterated variants. [b] from reference.[13b]

II. DFT investigations on hypothetical CO_2 evolution catalysed by 22

In this section, we explore the possibility of **22** to catalyse CO_2 formation from methanol. For the WGSR part, a stoichiometric amount of water would be needed, which, under the strongly basic conditions, would be deprotonated to afford hydroxide (cf. eq 4, driving force computed at the B97-D2/ECP3 level). In the original Cole-Hamilton system NaOH was added as base directly,[12] therefore we will use OH^- as reactant in our study.

$$H_2O + MeO^- \rightarrow MeOH + OH^-,\ \Delta G = -19.3\ kJ/mol \quad (4)$$

We considered three catalytic cycles, labelled ***Cycle-1***, ***Cycle-2*** and ***Cycle-3*** (see Scheme 6), all affording hydrogen and carbon dioxide via the following overall reaction (with ΔG computed at the ECP3 level):

$$2\ MeOH + OH^- \rightarrow 3\ H_2 + CO_2 + MeO^-,\quad \Delta G = 30.7\ kJ/mol \quad (5)$$

We first investigate the WGSR (pathway **I**), that would allow closing of the overall catalytic cycle for the full decomposition of methanol (see step *iii.* of ***Cycle-1*** in Scheme 6), as expected in the case of ethanol dehydrogenation catalysed by $[Rh(bipy)_2]Cl_2$.[9] Next, we considered the GDP mechanism, where the nucleophilic attack of the base takes place at the coordinated HCHO rather than at the carbonyl ligand (pathways J_A–J_B and J'_A–J'_B). In the production of MMA from methanol and methylpropanoate (MEP) catalysed by **22**, deprotonated MEP is proposed to attack coordinated formaldehyde in the presence of coordinated CO.[13]

Water gas shift reaction (WGSR) involving 22 (pathway I)

From the base and any traces of water that might be present, OH^- would form, which, after nucleophilic attack at the CO ligand could afford a metallacarboxylic acid intermediate that

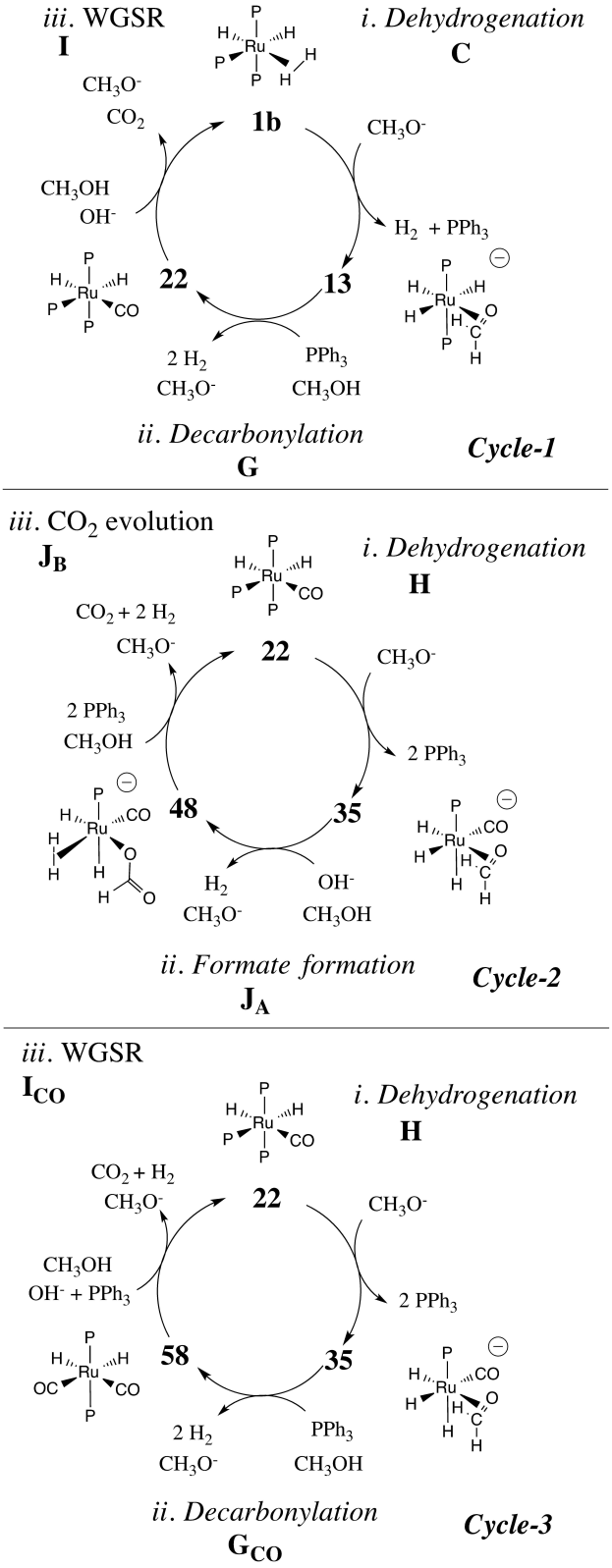

Scheme 6. Simplified overall catalytic cycles for the full decomposition of methanol catalysed by **1 b** (namely ***Cycle-1***; *top*) or **22** (namely ***Cycle-2*** *middle* and ***Cycle-3*** *bottom*), showing the sequences of pathways **C**, **G** and **I** (**Cycle 1**), **H**, $\mathbf{J_A}$ and $\mathbf{J_B}$ (**Cycle-2**) and **H**, $\mathbf{G_{CO}}$ and $\mathbf{I_{CO}}$ (***Cycle-3***). P=PPh_3.

eventually releases CO_2. Such reactivity is well-known for parent Ru carbonyl complexes,[19] and is considered herein in the present system. Such OH^- attack on **22** would afford **38** (Figure 3a). After decarboxylation and protonation, neutral **1b** could be re-formed, re-connecting to the dehydrogenation cycles promoted by this catalyst. A variety of pathways were trialled computationally to investigate the possibility of an intramolecular transfer of the –COOH hydrogen to the metal (see discussion on paths $\mathbf{I_a}$, $\mathbf{I_b}$ and $\mathbf{I_c}$ in section II.3 in the ESI, and related Figure S2 and Table S4), but such processes turn out to be less favourable than the solvent-mediated proton transfers shown in pathway **I** (Figure 3). This feature points to a low acidity of **38**, in keeping the wide range of pK_a observed for hydroxycarbonyl complexes, depending on the nature of the metal and of ancillary ligands.[20]

Surprisingly, this route turned out to be extremely endergonic with a prohibitively high barrier ($\Delta G^{\neq}$ [**22**→$\mathbf{TS_{40–41}}$] is 191.9 kJ/mol at the ECP2 level and 184.5 kJ/mol at the ECP3 level; see Figure 3c and Table 1, respectively). The main reason is that the initial uptake of OH^- to form the metalla-acid **38** is highly unfavourable ($\Delta G = 152.0$ kJ/mol; see Figure 3 and Table S3), with the barriers of the subsequent steps adding to the overall kinetic hindrance. Considering that "naked" OH^- might only be poorly described by a continuum model, we explored adding explicit MeOH solvent molecules or a counterion, Na^+ in this case (see Sections II.2 and II.3 in the ESI, and related Figure S3 and Table S5). The latter proved to have a stabilizing effect on the energetics of the initial nucleophilic attack, but even in this case (i.e. using NaOH as nucleophile), the resulting intermediate **38**·Na^+ is still endergonic by 95.5 kJ/mol (light grey curve in Figure 3c). If a similar stabilisation by counterions of *ca.* 32.2 kJ/mol would apply to all subsequent steps, the overall barrier via $\mathbf{TS_{40–41}}$ would still exceed 150 kJ/mol. As this stabilisation by the counterion in form of contact ion pairs is likely to be overestimated in these model complexes (in solution solvent-separated ion pairs with rather weaker cation-anion interactions are to be expected), it appears that the hypothesised WGSR is not viable, in accord with the lack of CO_2 evolution occurring with **22** as catalyst.[9]

Also, taking together pathways **C**, **G** and **I** to give ***Cycle-1*** (see Scheme 6), the overall free energy span is as high as 207.6 kJ/mol (see Table 1), thus indicating that the full decomposition of methanol should not be achievable *via* this route.

Full decomposition of methanol following the Gem-Diolate Pathway (GDP): Cycle-2.

Inspired by recent studies of Beller and co-workers,[10] we investigated another possibility to afford CO_2 and H_2 from methanol, via the formation of a gem-diol intermediate, as schematically described in Scheme 2. Again, complex **22** could be a starting point of a such mechanism, and could afford complex **35**, in which HCHO is π-coordinated to the metal, *i.e.* following the first steps of pathway **H** (see Figure 1). Then, OH^- attack on the coordinated HCHO could be envisaged, to afford the dianionic gem-diolate intermediate **43** (see Figure 4). After

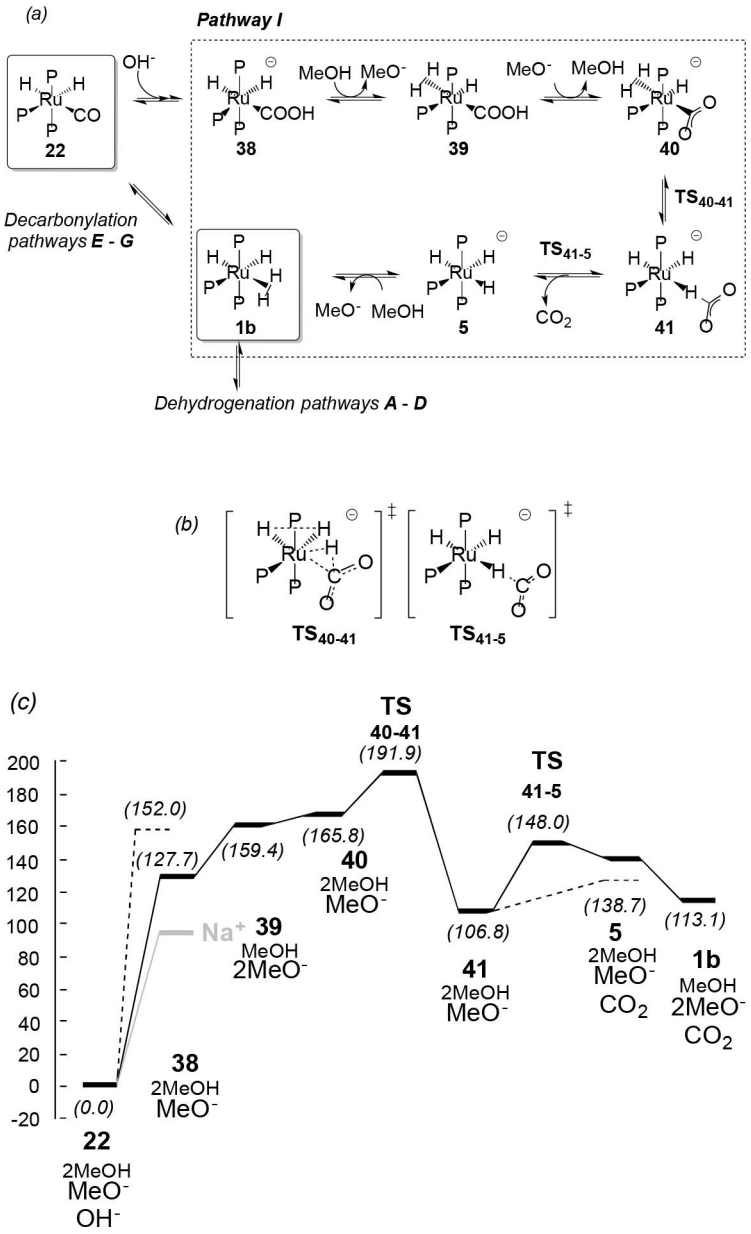

Figure 3. Reaction pathway **I**; schematic representation of: *(a)* intermediates *(b)* transition states (P = PPh_3) and *(c)* free-energy profile [kJ/mol], with calculations carried at the B97-D2/ECP2 level of theory using methanol as the model solvent. The light grey lines indicate inclusion of a counterion (see text). Relative free energies (without correction for BSSE), using **27** as reference, are given in parentheses. Reaction energies for every individual step are given in Table S3.

protonation (by methanol; to afford **44**) and liberation of H_2, β-H abstraction at the gem-diolate moiety affords formic acid, π-coordinated to the metal (in complex **46**). Then, transfer of the acidic proton of the HCOOH ligand to the metal can be mediated by the base (*e.g. via* a transient dianionic complex **47**), to finally afford the dihydrogen complex **48** featuring a formato ligand (see Pathway $\mathbf{J_A}$ in Figure 4). Subsequent CO_2 evolution proceeds via pathway $\mathbf{J_B}$ (see Figure 5), and requires a prior reorganisation of the formato ligand, where concerted Ru–O bond breaking and Ru–H coordination afford **49** via $\mathbf{TS_{48–49}}$. CO_2 release takes place via elongation of the H–C bond, up to full dissociation. This process follows the reverse reaction sequence reported in reference[21] in the case of CO_2 hydrogenation to formic acid. The resulting complex **50** is a "non-classical" pentahydride, from which H_2 decoordinates to afford **37**. The following reaction steps, regenerating complex **22**, are identical to those previously described in Pathway **H** (see Figure 1).

The reaction profiles computed for these two pathways ($\mathbf{J_A}$ and $\mathbf{J_B}$) indicate that OH^- uptake is again enderogonic (by 37.0 kJ.mol^{-1}; see Figure 4), and so are the subsequent H_2 dissociation and β-H transfer steps. Conversely, proton exchange from **46** to afford **48** is significantly exergonic (by 123.2 kJ.mol^{-1}). Calculations at the ECP3 level (see Table 1)

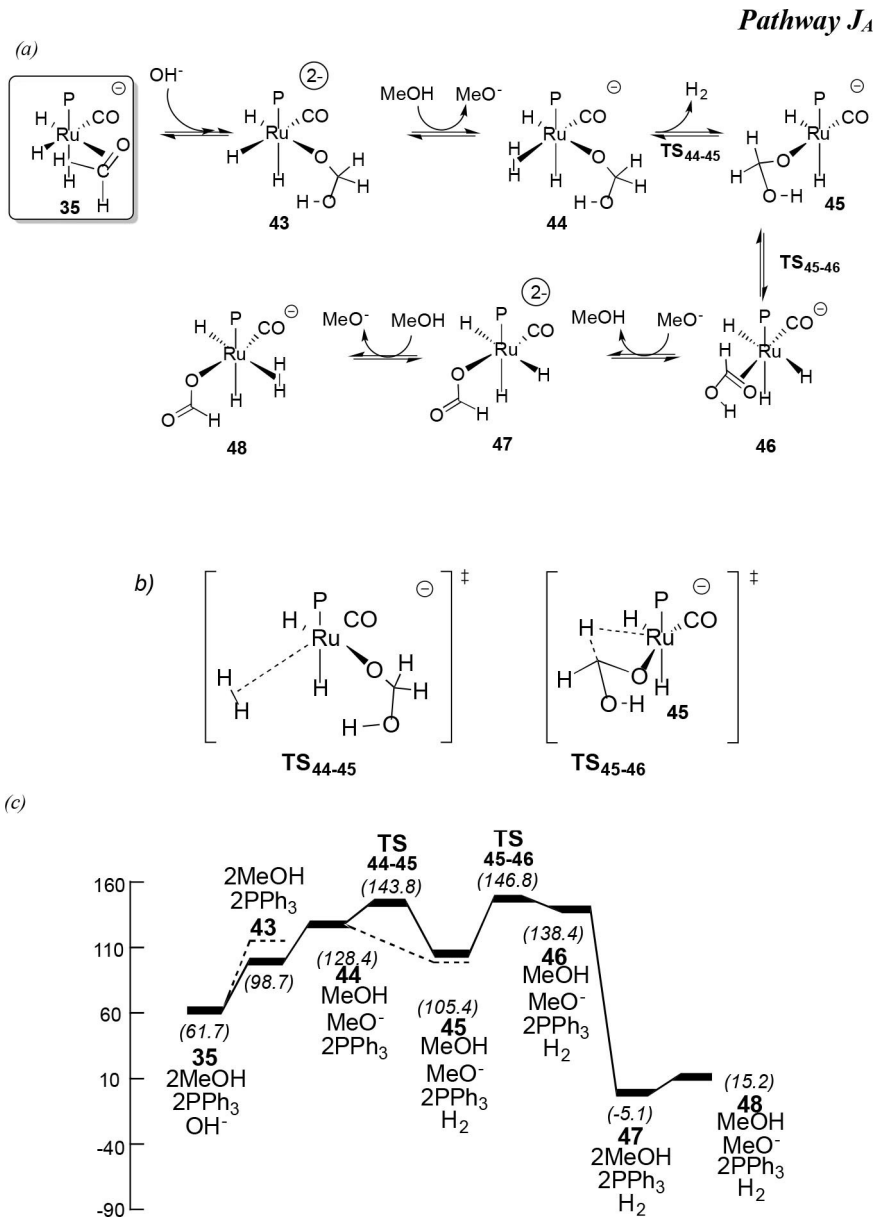

Figure 4. Pathway J_A: Schematic representation of: *(a)* intermediates and *(b)* transition states; *(c)* free-energy profile [kJ.mol^{-1}], with calculations carried at the B97-D2/ECP2 level of theory using methanol as the model solvent. The dashed lines indicate BSSE-corrected free energies. Relative free energies (without correction for BSSE), using **27** as reference, are given in parentheses. Reaction energies for every individual step are given in Table S6.

show that the overall activation barrier for **Cycle-2** is 166.1 kJ/mol, and corresponds to loss of H_2 from **44**. As a result, this pathway should not be viable kinetically, indicating that **22** is little active for full methanol decomposition via a GDP mechanism (**Cycle-2**). The analogous pathway **Cycle-2′**, involving isomers, is computed even less favourable (see paths **J′$_A$** and **J′$_B$** in the SI, in Figures S4–S5 and Table S6), with an overall activation barrier of 180.2 kJ/mol (see Table 1).

III. Full decomposition of methanol involving dicarbonyl complexes as intermediates (Cycle-3)

Taking together that the decoordination of HCHO from complex **35** in pathway **H** (or **35 ax** in pathway **H′**) is both kinetically and thermodynamically difficult (they are the intermediates right before the rate-limiting barrier), and that a new decarbonylation reaction may be envisaged at this stage, we investigated the possibility that dicarbonyl complexes could be involved to potentially catalyse the formation of CO_2.

The resulting pathway (referred to as **Cycle-3** in the following) is composed of three parts (namely, **H**, **G$_{CO}$** and **I$_{CO}$**; see Scheme 6), and would allow for full decomposition of

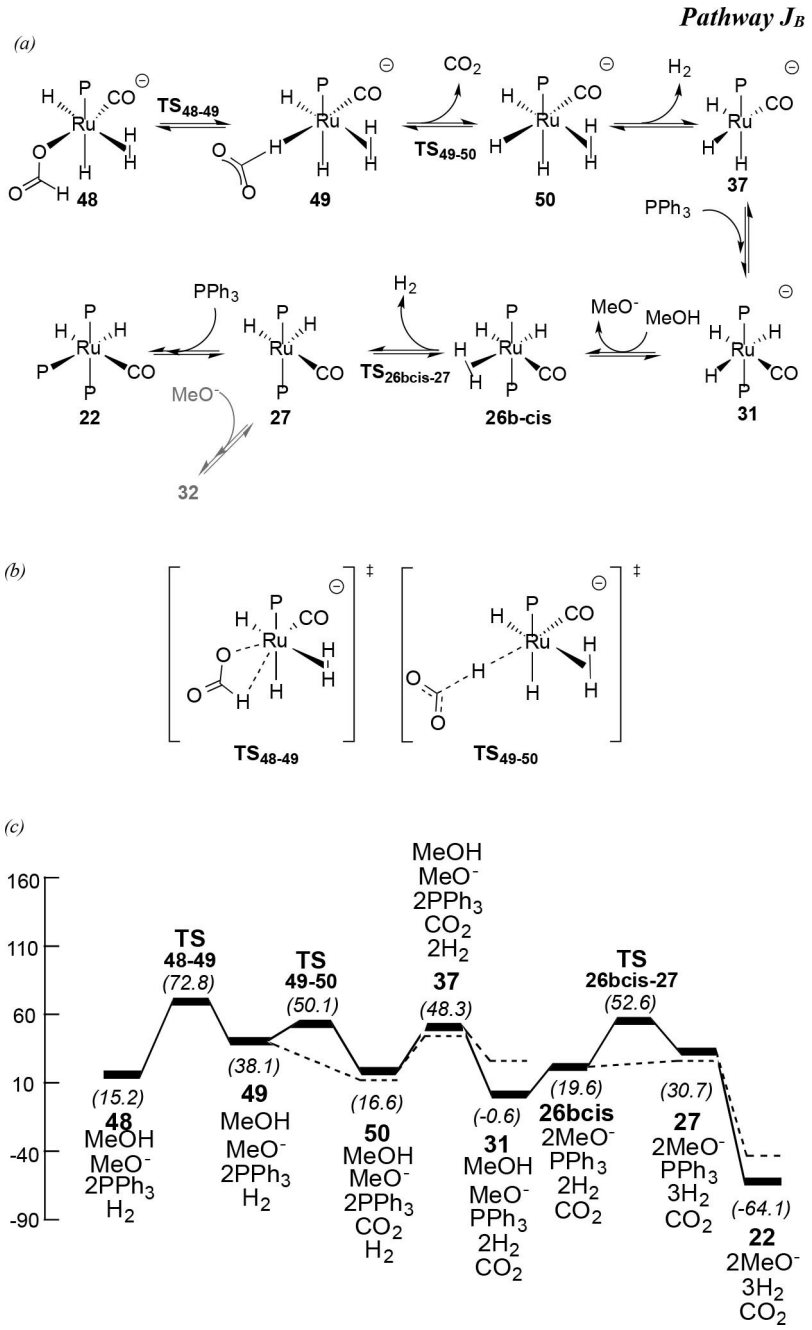

Figure 5. Pathway J_B: Schematic representation of: *(a)* intermediates and *(b)* transition states; *(c)* free-energy profile [kJ.mol^{-1}], with calculations carried at the B97-D2/ECP2 level of theory using methanol as the model solvent. The dashed lines indicate BSSE-corrected free energies. Relative free energies (without correction for BSSE), using **27** as reference, are given in parentheses. Reaction energies for every individual step are given in Table S6.

methanol. The latter are fully described in Supporting Information (see section II.5 and Figures S6–S10 and Table S7). For the complete cycle, **55** is indicated to be the TOF-determining intermediate (according to Shaik's energy span analysis),[22] and the highest point (the TOF-determining transition state) is formation of the acyl intermediate on the decarbonylation leg $\mathbf{G}_{CO}$ (via $\mathbf{TS}_{51\text{-}52}$). This raises the total energy span for **Cycle-3** to 208.1 kJ/mol (Table 1). The energy span of the analogous mechanism involving **H**′, $\mathbf{G}'_{CO}$ and $\mathbf{I}'_{CO}$ (labelled **Cycle-3**′) is similar, albeit slightly smaller (197.2 kJ/mol, see Table 1). Thus, the full decomposition of methanol *via* these routes should be very slow, indicating that **22** should not be very active for that process in the present catalytic system.

Discussion and Conclusions

We report a comprehensive DFT study of the reactivity of **22** in the context of H_2 generation from methanol. Its potential role in dehydrogenation, decarbonylation and water gas shift have

been carefully investigated. We have presented detailed reaction pathways for these processes, thus completing further the overall picture of the reactivity of this system.[13]

First, DFT calculations, supported by KIE measurements, show that partial dehydrogenation of methanol can effectively be catalysed by **22**. The activity of **22** as catalyst should be very similar to that of **1b**, as comparable overall activation barriers are obtained for the two corresponding mechanisms (in the range of ca. 112–131 kJ/mol; compare **C** and **H** in Table 1). Interestingly, dissociations of phosphine ligands are key steps in pathways **C** and **H**, so that bis- and mono- phosphine complexes are predicted to be active species. Phosphine dissociation processes are generally reasonably endergonic (e.g. 52.3 kJ/mol for PPh_3 dissociation from **22**, whereas PPh_3 dissociation from **32** is slightly exergonic, by −9.7 kJ/mol, because it is concomitant to a reorganisation of the first coordination sphere of Ru), resulting in the formation of di- and mono- phosphine intermediates. This feature is reminiscent of previous DFT studies where, *e.g.* low-ligated Pd(0), possessing a single phosphine as ancillary ligand, are predicted to be the active species, undergoing oxidative addition reactions.[23] Also, a direct comparison between catalytic cycles involving either mono- or bis- ligated triphenylphosphine-rhodium complexes has been reported for the parent hydroformylation reaction, showing that mono-phosphine complexes are more active.[24]

When **22** is considered as (pre)catalyst, the decarbonylation reaction (following pathway $\mathbf{G_{CO}}$) is found to be competitive to dehydrogenation (111.2 kJ/mol vs 115.7 kJ/mol for dehydrogenation via **H′** and decarbonylation via $\mathbf{G_{CO}}$, see Table 1). A similar feature was obtained in our previous study (involving **1b** as precatalyst).[13b] The latter reaction affords dicarbonyl complexes, namely the anionic trihidride **55** and the neutral dihydride **58**. Both are found to be relatively low-lying intermediates on the reaction profile (see Figure S6 and initiation Free energies reported in Table 1). We note that ruthenium(II) diphosphine dicarbonyl complexes can be readily synthetized and characterized by IR spectroscopy.[25] Additionally, the intermediacy of di- and tri- carbonyl complexes has been proposed, recently, in the dehydrogenation of formic acid.[26] However, such di- (or tri-)carbonyl complexes are not detected experimentally (under turnover conditions) in the system studied herein, presumably because the formation of **58** and **58ax** from **22** exhibit only very small driving forces (namely, −13.9 kJ/mol and −6.8 kJ/mol, respectively, see Table 1). As a result, there is no "thermodynamic sink" corresponding to their formation, and the latter complexes are therefore expected to be present in very low concentration. In contrast, a strong driving force was obtained for the formation of **22** from **1b** (−84.5 kJ/mol, *via* **1b** + MeOH → **22** + 3 H_2).[13b] **22** is therefore expected to be more populated than **58** (or **58ax**), so that its characterisation becomes achievable. However, the catalytic activity of these low-coordinated phosphine complexes for full methanol dehydrogenation is found to be too low (*vide infra*).

We have investigated two WGSR pathways, starting either from the mono-carbonyl (namely **22**; see pathway **I**) or dicarbonyl complexes (namely **58**; see Pathway $\mathbf{I_{CO}}$). Significantly higher barriers are computed for these processes compared to dehydrogenation and decarbonylation. We found that the main factor preventing the reaction is a large thermodynamic hindrance for OH^- attack on the coordinated CO, which is the very first step of the WGSR. Uptake of OH^- by **22** and **58** is predicted to be endergonic by 152.0 kJ/mol and 90.2 kJ/mol, respectively (Figures 3 and S8, respectively). As a result, the WGSR reaction could not be achieved in this system, even though it is well known in parent Rh[9] or Ru[19] complexes. Some of us recently showed that the formation of metallacarboxylic acids through OH^- attack on [$\mathbf{L_nM}$(CO)] complexes (**M** = Fe, Ru, Os, and **L** = CO, PMe_3, PF_3, py, bipy, Cl, H) can exhibit a large span of driving forces ($\Delta G = -144$ kJ/mol to $+122$ kJ/mol).[27] The π-acidity of the co-ligands has been recognized as a key factor in the process, and the more electron-withdrawing ligands were predicted to favour OH^- uptake.[27] Because the WGSR pathways are unfavourable, the resulting cycles for full dehydrogenation of methanol and water, ***Cycle-1*** or ***Cycle-3*** (Scheme 6), have prohibitively high overall activation barriers (between 197.2 and 208.1 kJ/mol, see values for ***Cycle-1***, ***Cycle-3*** and ***Cycle-3′*** in Table 1). The similar barriers observed between ***Cycle-1*** and ***Cycle-3*** indicates that substituting PPh_3 by CO in the precatalyst is not beneficial for the process.

Nucleophilic attack at coordinated HCHO (e.g. in **35**) is not kinetically viable either, so that CO_2 evolution *via* a gem-diolate intermediate (namely **43**), as anticipated in other Ru complexes,[10] could not be expected as well. Our DFT results are therefore consistent with the lack of CO_2 evolution with (pre)catalysts **1b** and **22**. We note, however, that the overall cycle for full methanol dehydrogenation has a significantly lower overall barrier when involving such a GDP route (***Cycle-2*** in Scheme 6, overall barrier 166.1 kJ/mol, see Table 1) as compared to cycles involving WGSRs (***Cycle-1*** and ***Cycle-3,*** overall barriers exceeding 197 kJ/mol, see Table 1). If, through appropriate ligand design, the barrier of the GDP route could be lowered by some 30 kJ/mol without compromising the viability of the dehydrogenation pathways, a one-pot catalyst for full methanol dehydrogenation based on the Cole-Hamilton system might be within reach. Calculations along these lines are in progress.

To summarize, the new mechanistic insights presented herein emphasise the extreme complexity of this catalytic system, where many competitive reaction channels (including many "crossings" and, sometimes, "dead-ends") are encountered to afford H_2 generation. Our main results are: *i)* **22** should be active as a methanol dehydrogenation catalyst, and its activity should be comparable to that of **1b**, as is observed experimentally.[11] Also, a detailed reaction mechanism for the process has been elucidated and is supported by KIE measurements. *ii)* The lack of CO_2 evolution in this system has been rationalised by the fact that neither coordinated CO nor HCHO ligands are electrophilic enough to undergo attack by the base (OH^-). As a result, neither WGSR nor GDP reactions are viable. As a result, the full decomposition of methanol, as schematically described in Scheme 2, cannot be achieved with the original, Cole-Hamilton catalyst, in keeping with experimental findings.[9] We hope that this study will stimulate further development of

this interesting system, including the rational design of new ligands, and further theoretical and experimental mechanistic studies. Beyond the case of the Ru/PPh_3 complexes presented here, our results may also be useful better to understand the reactivity of analogous dehydrogenation catalysts,[2–3] that may exhibit similar reactivity.

Experimental Section

General materials, methods and instruments

All manipulations and reactions were carried out under N_2 gas (dried through a Cr(II)/silica packed glass column) using different techniques including a standard Schlenk, vacuum line and a glove box. Solvents were dried and degassed prior to use. [RuH_2(CO)(PPh_3)$_3$] (**22**), *t*-OBuNa, methanol, methanol-d_4 and *tert*-butyl propanoate were purchased from Sigma-Aldrich. *tert*-Butyl propanoate was dried over Na_2SO_4 and distilled under dinitrogen. Na_2CO_3 (anhydrous) was purchased from Fisher Scientific.

Toluene was dried using a Braun Solvent Purification System. Methanol was dried and degassed by distillation from magnesium under dinitrogen. All gases were purchased from BOC gases.

GC-MS analyses were performed using a Hewlett Packard 6890 series GC system equipped with an Agilent J&W HP-1 column capillary (30.0 m × 248 μm × 0.25 μm nominal). Method: flow rate 0.8 mL min^{-1} (He carrier gas), split ratio 100 : 1, starting temperature 50 °C (4 min) ramp rate 20 °C min^{-1} to 130 °C (2 min), ramp rate 20 °C min^{-1} to 280 °C (15.50 min). Qualitative analyses were performed using an HP5973 mass selective detector (GC-MS).

Determination of KIE's

A Hastelloy™ autoclave was fitted with a magnetic stirrer and charged under a dinitrogen atmosphere with catalyst 1 (0.124 g, 0.135 mmol) and *t*-BuONa (2.6 g, 27.0 mmol). Toluene (10 mL) and *t*-BuP (15.64 mL, 103.9 mmol) were added through the injection port together with methanol (3.8 mL, 93.5 mmol), methanol-d_4 (3.8 mL, 93.5 mmol) and 2,4-dimethyl-6-tert-butylphenol (Topanol A, 0.01 mL, in order to prevent MMA polymerisation). The autoclave was sealed, pressurised with ethene (6 bar) and heated to 170 °C for 3 hours. The autoclave was then cooled to room temperature, vented to the atmosphere and the obtained product mixture analysed by GC-MS spectroscopy.

Computational Details

The exact same computational protocol as in our two previous studies has been employed herein.[13] The latter has been previously described and validated.[28] Briefly, geometry optimizations are performed at the BP86 level with a medium-sized basis set, then energies are refined with a larger basis set and a dispersion-corrected functional[29] in order to account for the critical non-covalent interactions involved when bulky ligands are considered.[30] This protocol has been successfully employed to model catalytic systems involving Ru[13] and Rh[31] complexes with voluminous triphenylphosphine ligands. We also performed additional methodological tests herein to further validate our protocol (see Section IV in Supporting Information). Briefly, the following steps are involved:

Geometries and thermodynamic corrections

Geometries of all complexes were fully optimized at the RI-BP86/ECP1 level, *i.e.* employing the exchange and correlation functionals of Becke[32] and Perdew,[33] respectively, in conjunction with the SDD basis on Ru, denoting the small-core Stuttgart-Dresden relativistic effective core potential (ECP) together with its valence basis set,[34] and the standard 6–31G(d,p) basis for all other elements, except for the carbon and hydrogen atoms of the phenyl rings for which a smaller 3-21G basis set were employed, and suitable auxiliary basis sets for the fitting of the Coulomb potential.[35] Harmonic frequencies were computed analytically and were used without scaling to obtain enthalpic and entropic corrections at the experimentally used temperature of 150 °C.[12] The corresponding correction terms δE_G were estimated at the RI-BP86/ECP1 level and have been obtained as the difference of the reaction energy of a given step ($\Delta E_{RI-BP86/ECP1}$) and the corresponding free energy ($\Delta G_{RI-BP86/ECP1}$), Eq. (6):

$$\delta E_G = \Delta G_{RI\text{-}BP86/ECP1} - \Delta E_{RI\text{-}BP86/ECP1} \quad (6)$$

The entropic contributions have been evaluated at a pressure of 1354 atm in order to model the changes in entropy for a condensed phase.[36] This approach has been validated in Ref,[28] where we showed that such an increased pressure allows for the modelling of binding entropies in CH_2Cl_2 in excellent accord with the experiment. The corresponding correction terms (δE_G) for each step of the catalytic cycles are gathered in Tables S1 and S3–S7 along with other correction terms *(vide infra)*.

The transition states (denoted $\mathbf{TS_{x-y}}$) were characterized by a single imaginary frequency and visual inspection of the corresponding vibrational mode ensured that the desired minima **x** and **y** were connected. The reaction pathways have been investigated more closely by following the Intrinsic Reaction Coordinate (IRC)[37] starting from $\mathbf{TS_{x-y}}$ and leading to the intermediates **x** and **y**.

The initial structures of the complexes were constructed by hand and were derived from structures stemming from our previous studies,[13] following the reaction path.

Refined energies

Refined energies were obtained from single-point calculations (on the RI-BP86/ECP1 geometries) using the same SDD ECP on Ru[34] and a larger basis set (hereafter noted ECP2), namely 6-311 + G(d,p), on all elements except for the carbon and hydrogen atoms of the phenyl rings, for which the 6-31G(d,p) basis set was used. The refined energies are computed with the B97-D2 functional,[29] that follows the DFT–D2 general approach of Grimme,[29,38] in which the functional energies are corrected by an atomic pair-wise additive term accounting for the long-range non-covalent interactions. B97-D2 has been successfully employed to study Ru[13,39] and Rh[31,40] catalysed reactions, and has been recently shown to perform well at describing several "bulky" transition metal-complexes.[41]

Energies have been corrected for the basis set superposition error (BSSE) using the counterpoise method.[42] The BSSE energy corrections are noted δE_{BSSE}. Estimates of the solvation effects were computed using the Conductor-like screening model (COSMO),[43] with a dielectric constant $\varepsilon = 32.63$ to model the experimentally used methanol solvent.[12] The δE_{solv} energy correction is defined as the difference between the reaction energy in the continuum (including the outlaying charge correction;[44] noted ΔE_{COSMO}) and in the gas phase (ΔE), at the B97-D2/ECP2 level, Eq. (7):

$$\delta E_{solv} = \Delta E_{COSMO} - \Delta E \quad (7)$$

Both counterpoise and COSMO corrections were calculated by performing single-point calculations at the B97-D2/ECP2 level on the RI-BP86/ECP1 geometries. The final ΔG values are calculated as a sum of all energy correction terms, added to the raw B97-D2/ECP2 gas phase reaction energies (ΔE), Eq. (8):

$$\Delta G = \Delta E + \delta E_{solv} + \delta E_{BSSE} + \delta E_G \quad (8)$$

Where ΔE, δE_{solv} and δE_{BSSE} are computed at the B97-D2/ECP2 level and δE_G at the RI-BP86/ECP1 level (*vide supra*).

Refined free energies are given in Table 1. The latter involve calculations at the higher ECP3 level, consisting on using a larger basis set, where all P, O, C, and H atoms are described by the 6-311 + G(d,p) basis set (and the same SDD ECP on Ru). We also applied the protocol described in Ref. [13a] to correct free energies for BSSE when more than one ligand are coordinated/decoordinated during a given reaction. Technical details on these calculations are given in section II.2 in Supporting Information.

All RI-BP86 calculations have been performed with the Gaussian09 software,[45] whereas B97-D2 (gas phase and COSMO) calculations were performed with the Turbomole package.[46]

Acknowledgements

We wish to thank Lucite International for a studentship (P.L.) and EaStCHEM for support and access to the EaStCHEM Research Computing Facility. We also thank Dr. H. Früchtl for technical support. N.S. thanks the Univ. Grenoble Alpes, the CNRS and the ICMG FR 2607 for financial support. The Pcecic and Froggy platforms of the CIMENT infrastructure (ICMG FR 2607) are also acknowledged (project "liqsim"). The research data underpinning this publication can be accessed at https://doi.org/10.17630/f5878980-a407-4b92-b4db-f14dbe3e9afc.

Conflict of Interest

The authors declare no conflict of interest.

Keywords: Hydrogen generation · Ruthenium · Carbonyl complexes · Reaction mechanisms · DFT

[1] a) N. Taccardi, D. Assenbaum, M. E. M. Berger, A. Bosmann, F. Enzenberger, R. Wolfel, S. Neuendorf, V. Goeke, N. Schodel, H. J. Maass, H. Kistenmacher, P. Wasserscheid, *Green Chem.* **2010**, *12*, 1150–1156; b) Y. Zhan, Y. Shen, S. Li, B. Yue, X. Zhou, *Chem. Commun.* **2017**, *53*, 4230–4233; c) Y. Li, P. Sponholz, M. Nielsen, H. Junge, M. Beller, *ChemSusChem* **2015**, *8*, 804–808.
[2] a) A. K. Singh, S. Singh, A. Kumar, *Catal. Sci. Technol.* **2016**, *6*, 12–40; b) K. Sordakis, C. Tang, L. K. Vogt, H. Junge, P. J. Dyson, M. Beller, G. Laurenczy, *Chem. Rev.* **2018**, *118*, 372–433.
[3] a) M. Trincado, D. Banerjee, H. Grutzmacher, *Energy Environ. Sci.* **2014**, *7*, 2464–2503; b) R. H. Crabtree, *Chem. Rev.* **2017**.
[4] E. Alberico, M. Nielsen, *Chem. Commun.* **2015**, *51*, 6714–6725.
[5] a) J. K. MacDougall, D. J. Cole-Hamilton, *Polyhedron* **1990**, *9*, 1235–1236; b) J. Zhang, M. Gandelman, L. J. W. Shimon, D. Milstein, *Dalton Trans.* **2007**, 107–113.
[6] E. Delgado-Lieta, M. A. Luke, R. F. Jones, D. J. Cole-Hamilton, *Polyhedron* **1982**, *1*, 839–840.
[7] M. Kilner, D. V. Tyers, S. P. Crabtree, M. A. Wood, *U. S. Patent WO03093208* **2003**.
[8] NIST database: https://webbook.nist.gov/chemistry/ (last accessed: March **2020**).
[9] D. Morton, D. J. Cole-Hamilton, I. D. Utuk, M. Paneque-Sosa, M. Lopez-Poveda, *J. Chem. Soc. Dalton Trans.* **1989**, 489–495.
[10] a) M. Nielsen, E. Alberico, W. Baumann, H.-J. Drexler, H. Junge, S. Gladiali, M. Beller, *Nature* **2013**, *495*, 85–89; b) E. Alberico, A. J. J. Lennox, L. K. Vogt, H. Jiao, W. Baumann, H.-J. Drexler, M. Nielsen, A. Spannenberg, M. P. Checinski, H. Junge, M. Beller, *J. Am. Chem. Soc.* **2016**, *138*, 14890–14904.
[11] R. E. Rodríguez-Lugo, M. Trincado, M. Vogt, F. Tewes, G. Santiso-Quinones, H. Grützmacher, *Nat. Chem.* **2013**, *5*, 342–347.
[12] D. Morton, D. J. Cole-Hamilton, *J. Chem. Soc. Chem. Commun.* **1988**, 1154–1156.
[13] a) N. Sieffert, M. Bühl, *J. Am. Chem. Soc.* **2010**, *132*, 8056–8070; b) N. Sieffert, R. Réocreux, P. Lorusso, D. J. Cole-Hamilton, M. Bühl, *Chem. Eur. J.* **2014**, *20*, 4141–4155.
[14] P. Lorusso, G. R. Eastham, D. J. Cole-Hamilton, *Dalton Trans.* **2018**, *47*, 9411–9417.
[15] For instance, the isomerisation of the hexa-coordinated complex **35** into **35ax** is found to be activated by 77.2 kJ/mol (at the B97-D2/ECP2 level, without BSSE correction), which should be surmountable under reaction conditions (at 423 K). Free energy barriers for isomerisation of five-coordinated complexes are expected to be even lower.
[16] Note that the protonated analogue $[RuCl_2(CO)(PPh_3)_2(MeOH)]$ complex has been characterized by X-ray diffraction, see: A.-Q. Jia, Q. Ma, H.-T. Shi, Q. Chen, W.-H. Leung, Q.-F. Zhang, *Inorg. Chim. Acta* **2012**, *392*, 99.
[17] P. Lorusso, J. Coetzee, G. R. Eastham, D. J. Cole-Hamilton, *ChemCatChem* **2016**, *8*, 222–227.
[18] M. Gomez-Gallego, M. A. Sierra, *Chem. Rev.* **2011**, *111*, 4857–4963.
[19] H. Ishida, K. Tanaka, M. Morimoto, T. Tanaka, *Organometallics* **1986**, *5*, 724–730.
[20] C. Creutz, *Carbon Dioxide Binding to Transition-Metal Centers* (Ed. Elsevier), B. P. Sullivan, K. Krist, H. E. Guard, **2012**, p19.
[21] A. Urakawa, F. Jutz, G. Laurenczy, A. Baiker, *Chem. Eur. J.* **2007**, *13*, 3886–3899.
[22] S. Kozuch, S. Shaik, *Acc. Chem. Res.* **2011**, *44*, 101–110.
[23] M. Ahlquist, P. Fristrup, D. Tanner, P.-O. Norrby, *Organometallics* **2006**, *25*, 2066–2073.
[24] I. Jacobs, B. de Bruin, J. N. H. Reek, *ChemCatChem* **2015**, *7*, 1708–1718.
[25] J. Chatt, B. L. Shaw, A. E. Field, *J. Chem. Soc.* **1964**, 3466.
[26] M. Czaun, A. Goeppert, J. Kothandaraman, R. B. May, R. Haiges, G. K. S. Prakash, G. A. Olah, *ACS Catal.* **2014**, *4*, 311–320.
[27] S. Ahmad, E. A. Berry, C. H. Boyle, C. G. Hudson, O. W. Ireland, E. A. Thompson, M. Bühl, *J. Mol. Model.* **2019**, *25*, 45.
[28] N. Sieffert, M. Bühl, *Inorg. Chem.* **2009**, *48*, 4622–4624.
[29] S. Grimme, *J. Comput. Chem.* **2006**, *27*, 1787–1799.
[30] See e.g.: a) Y. Zhao, D. G. Truhlar, *Org. Lett.* **2007**, *9*, 1967; b) Y. Zhao, D. G. Truhlar, *J. Chem. Theory Comput.* **2009**, *5*, 324; c) N. Sieffert, M. Bühl, *Inorg. Chem.* **2009**, *48*, 4622; d) Y. Minenkov, G. Occhipinti, V. R. Jensen, *J. Phys. Chem. A* **2009**, *113*, 11833.
[31] J. A. Fuentes, P. Wawrzyniak, G. J. Roff, M. Buhl, M. L. Clarke, *Catal. Sci. Technol.* **2011**, *1*, 431–436.
[32] A. D. Becke, *Phys. Rev. A* **1988**, *38*, 3098.
[33] a) J. P. Perdew, *Phys. Rev. B* **1986**, *33*, 8822; b) J. P. Perdew, *Phys. Rev. B* **1986**, *34*, 7406.
[34] D. Andrae, U. Häußermann, M. Dolg, H. Stoll, H. Preuß, *Theor. Chim. Acta* **1990**, *77*, 123–141.
[35] Generated automatically according to the procedure implemented in Gaussian 09.
[36] Following the argument in R. L. Martin, P. J. Hay, L. R. Pratt, *J. Phys. Chem. A* **1998**, *102*, 3565–3573, where this simple procedure has been proposed as adjustment for the concentration of water molecules in the liquid, and where the necessary value for the pressure has been derived from the experimental density of liquid water. Such an elevated pressure is designed to model the change in entropy existing in condensed phase when the number of particle vary during a given reaction.
[37] a) C. Gonzalez, H. B. Schlegel, *J. Chem. Phys.* **1989**, *90*, 2154–2161; b) C. Gonzalez, H. B. Schlegel, *J. Phys. Chem.* **1990**, *94*, 5523–5527.
[38] S. Grimme, *J. Comput. Chem.* **2004**, *25*, 1463–1473.

[39] M. Piacenza, I. Hyla-Kryspin, S. Grimme, *J. Comput. Chem.* **2007**, *28*, 2275–2285.
[40] N. Sieffert, J. Boisson, S. Py, *Chem. Eur. J.* **2015**, *21*, 9753–9768.
[41] Y. Minenkov, A. Singstad, G. Occhipinti, V. R. Jensen, *Dalton Trans.* **2012**, *41*, 5526–5541.
[42] S. F. Boys, F. Bernardi, *Mol. Phys.* **1970**, *19*, 553–566.
[43] A. Klamt, G. Schüürmann, *J. Chem. Soc. Perkin Trans. 2* **1993**, *5*, 799–805.
[44] A. Klamt, V. Jonas, *J. Chem. Phys.* **1996**, *105*, 9972–9981.
[45] Gaussian 09, Revision D.01, M. J. Frisch, G. W. Trucks, H. B. Schlegel, G. E. Scuseria, M. A. Robb, J. R. Cheeseman, G. Scalmani, V. Barone, B. Mennucci, G. A. Petersson, H. Nakatsuji, M. Caricato, X. Li, H. P. Hratchian, A. F. Izmaylov, J. Bloino, G. Zheng, J. L. Sonnenberg, M. Hada, M. Ehara, K. Toyota, R. Fukuda, J. Hasegawa, M. Ishida, T. Nakajima, Y. Honda, O. Kitao, H. Nakai, T. Vreven, J. A. Montgomery Jr., J. E. Peralta, F. Ogliaro, M. Bearpark, J. J. Heyd, E. Brothers, K. N. Kudin, V. N. Staroverov, T. Keith, R. Kobayashi, J. Normand, K. Raghavachari, A. Rendell, J. C. Burant, S. S. Iyengar, J. Tomasi, M. Cossi, N. Rega, J. M. Millam, M. Klene, J. E. Knox, J. B. Cross, V. Bakken, C. Adamo, J. Jaramillo, R. Gomperts, R. E. Stratmann, O. Yazyev, A. J. Austin, R. Cammi, C. Pomelli, J. W. Ochterski, R. L. Martin, K. Morokuma, V. G. Zakrzewski, G. A. Voth, P. Salvador, J. J. Dannenberg, S. Dapprich, A. D. Daniels, O. Farkas, J. B. Foresman, J. V. Ortiz, J. Cioslowski, D. J. Fox, Gaussian, Inc., Pittsburgh, PA **2009**.
[46] a) R. Ahlrichs, M. Baer, M. Haeser, H. Horn, C. Koelmel, *Chem. Phys. Lett.*, **1989**, *162*, 165; b) O. Treutler, R. Ahlrichs, *J. Chem. Phys.* **1995**, *102*, 346; c) M. v Arnim, R. Ahlrichs, *J. Comb. Chem.* **1998**, *19*, 1746; d) TURBOMOLE V6.4 2012, a development of University of Karlsruhe and Forschungszentrum Karlsruhe GmbH **1989–2007**, TURBOMOLE GmbH, since 2007; available from http://www.turbomole.com (last accessed March 2020).

Manuscript received: January 29, 2020
Revised manuscript received: March 13, 2020
Accepted manuscript online: March 16, 2020
Version of record online: ■■, ■■■

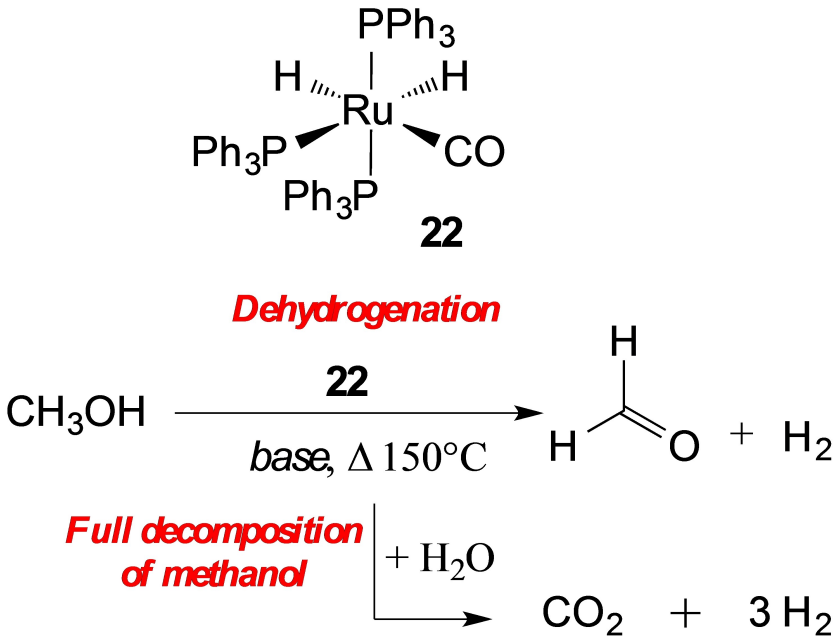

Dr. P. Lorusso, S. Ahmad, K. Brill , Prof. D. J. Cole-Hamilton, Dr. N. Sieffert, Prof. M. Bühl**

Reaction mechanisms: Using DFT calculations and measurements of kinetic isotope effects, the mechanism of $[RuH_2(PPh_3)_3(CO)]$ in catalytic acceptor-less dehydrogenation of methanol to formaldehyde was explored.